Chapter 6
The Effect of Nitrogen-Doped Mesoporous Carbon Spheres (NMCSs) on the Electrochemical Behavior of Carbon Steel in Simulated Concrete Pore Water

H. Mahmoud, J. Tang, Dessi A. Koleva, J. Liu, Y. Yamauchi, and M. Tade

Abstract The influence of highly nitrogen-doped mesoporous carbon spheres (NMCSs) (internal pore size of 5.4–16 nm) on the electrochemical response of low carbon steel (St37) in model alkaline solutions of pH 13.9 and 12.8 was studied, using Open Circuit Potential (OCP) monitoring, Electrochemical Impedance Spectroscopy (EIS) and Cyclic Voltammetry (CV). Prior to adding the NMCSs in the relevant solutions, they were characterized in the same model medium by measuring their Zeta-potential, hydrodynamic radius and particle size distribution, using dynamic light scattering (DLS) and transmission electron microscopy (TEM). In alkaline environment of pH 13.9 and 12.8, which simulates the concrete pore water of fresh and mature concrete, the DLS measurements indicated that the hydrodynamic radius of NMCSs particle varied from 296 nm to 183, respectively. According to the Zeta-potential measurements in the same solutions, the NMCSs were slightly positively charged.

H. Mahmoud (✉) • D.A. Koleva
Faculty of Civil Engineering and Geosciences, Delft University of Technology, Section of Materials and Environment, Stevinweg 1, 2628 CN Delft, The Netherlands
e-mail: H.AminHassan@tudelft.nl

J. Tang • Y. Yamauchi
National Institute for Materials Science (NIMS), 1-1 Namiki, Tsukuba, Ibaraki 305-0044, Japan

J. Liu • M. Tade
Curtin University of Technology, Faculty of Science and Engineering, Department of Chemical & Petroleum Engineering, GPO Box U1987, Perth, WA, Australia

L.E. Rendon Diaz Miron, D.A. Koleva (eds.), *Concrete Durability*,
DOI 10.1007/978-3-319-55463-1_6

The addition of 0.016 wt.% of NMCSs to the model medium induced certain variation in the electrochemical response of the tested steel. In alkaline solutions of pH 12.8, the presence of NMCSs in the passive film/solution interface induced a delay in the formation of a stable passive film. On the other hand, in solutions of pH 13.9, the higher corrosion activity on the steel surface, enhanced by high pH, was limited by adsorption of NMCSs on the film/substrate interface. In addition competing mechanisms of active state, i.e., enhanced oxidation on the one hand, and particles adsorption on anodic sites and oxidation limitation, on the other hand, was relevant in solution of pH 13.9 inducing larger fluctuations in impedance response and stabilization only towards the end of the testing period.

Except steel electrochemical response, the properties of the cement-based bulk matrix were investigated in the presence of the aforementioned additives. The mortar bulk matrix properties were highly affected by NMCSs. The lowest electrical resistivity values were recorded in mortar specimens with mixed-in 0.025 wt.% NMCSs (with respect to dry cement weight). Furthermore, the addition of 0.025 wt.% NMCSs increased the compressive strength when compared to control specimens. The presence of F127 as a dispersing agent for NMCSs was found to be not suitable for reinforced concrete applications, which is in view of the reduced mechanical strength and electrical resistivity of the cement-based bulk matrix. This is in addition to the adverse effect on the formation of electrochemically stable passive layer on steel surface in alkaline medium in its presence.

Keywords NMCSs • Steel corrosion • Alkaline solutions • Cement-based materials

6.1 General Introduction

Concrete is the most widely used construction material worldwide. It is considered to be a durable material; however, premature deterioration of reinforced concrete structures (RCS) can be induced by chloride ingress and/or carbonation [1–3]. The result is subsequent steel corrosion initiation and propagation, which significantly affect the RCS durability. Therefore, there is a constant drive to improve the properties of RCS, e.g., by tailoring tensile or flexural mechanical properties in order to achieve superior damage residence and increased RCS' durability [4, 5].

Corrosion of the steel reinforcement is widely recognized to be the main cause for RCS durability loss [6–8], reflected by the enormous economic consequences from maintenance and repair [3]. Over the last decade there has been a rapid growth in the diversity of applied methods to improve RCS durability by minimizing or preventing corrosion of the steel reinforcement.

The state-of-the-art reports on numerous corrosion protection methods and approaches [9] such as: the introduction of alternative high corrosion resistant reinforcements [10], improving the concrete barrier properties [11–13], cathodic

protection [14, 15], corrosion inhibitors [16], electrochemical chloride extraction [15], protective coatings [17], etc. All these are meant to meet given requirements of serviceability, strength and stability throughout the designed service life of a reinforced concrete structure, without significant loss of utility or excessive unforeseen maintenance [18].

Many studies have been focused on the performance of cement-based composite materials incorporating allotropes of carbon, e.g., carbon nanotubes (CNTs), carbon nanofibers (CNFs) and graphene oxide, all of these generally used to improve the mechanical performance of cementitious materials [11, 12, 19]. However, the complete understanding of the mechanisms upon which these additions react with the cement-based materials and affect further the corrosion performance of the embedded steel is still a challenge.

In the frame of a recent approach to corrosion control in reinforced concrete using various nanomaterials, admixed within the cement-based composite, the possible application of nitrogen-doped mesoporous carbon spheres (NMCSs) was also considered. Keeping in mind the high surface area of NMCSs, including the expected alteration of electrical properties of the bulk material in their presence, several hypothetical applications were evaluated. For example, the NMCSs-modified cement-based bulk matrix would theoretically present a reduced electrical resistance. Hence, possible application for NMCSs in cement-based layers within cathodic protection systems, or control of stray current-induced corrosion in RCS, could be a novel and feasible approach.

The NMCSs showed high chemical inertness, high surface area (from 343 to 363 $m^2\ g^{-1}$) and large porosity (from 0.45 to 0.48 $cm^3\ g^{-1}$), good electrical conductivity and elevated electro-catalytic properties especially for oxygen reduction reactions [20–22]. With respect to the application of NMCSs in RCS, it should be noted that, within admixing of the NMCSs in cement-based composite materials, their dispersion in the bulk matrix is expected to be a critical parameter. This holds for carbon-based materials (as admixtures) in general and is expected to strongly influence the properties of the final cement-based composite [23]. One of the reasons for a potentially poor dispersion may be the cement particles agglomeration [24] and/or the tendency of carbon particles to agglomerate themselves due to the possible interference of attraction (Van der Waals) forces [25]. Different dispersion methods have been employed and reported for both aqueous (water and solutions) and solid (cement-based) medium [20, 23–26]. For example, in order to achieve homogenous dispersion of carbon nanomaterials in water, the use of various surfactants is generally employed [27, 28], together with or without ultrasonication [29]. In the present work, Pluronic F127 was used as a dispersing agent for NMCSs in the aqueous model medium [21, 30], while either ultrasonication or addition only of F127 was used for the solid (cement-based) environment.

Regarding the incorporation of NMCSs in reinforced concrete, certain effects on steel corrosion resistance, together with possibly superior concrete material properties, are expected. For example, improving mechanical properties, decreasing electrical resistivity, alteration in the bulk matrix properties and microstructure in terms

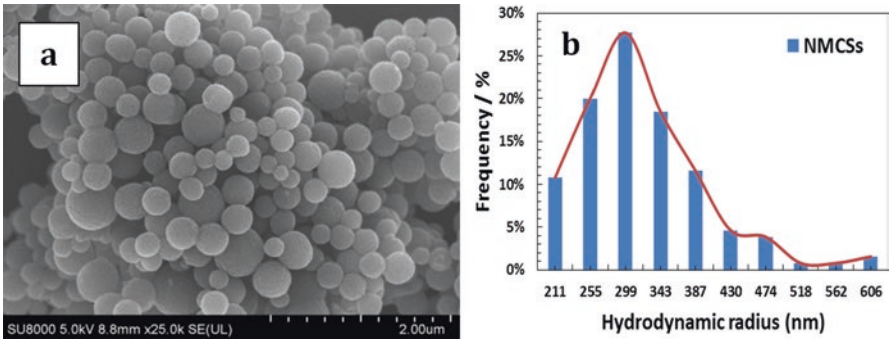

Fig. 6.1 Shows **a**) TEM image, and **b**) hydrodynamic radius distribution of as-recieved NMCSs particles

reduced porosity/permeability, etc. could be achieved. These in turn are also expected to lead to an increase of steel corrosion resistance.

This work briefly introduces results from tests on global cement-based material properties (mechanical and electrical properties of mortar) in the presence of 0.016 wt.% NMCSs. Next, the study aims to evaluate the effect of NMCSs on the electrochemical behavior of steel in model solution as an approach that normally precedes tests in reinforced mortar and concrete. Model solutions of NaOH were used, rather than complex simulated environment (as cement extract for example), in order to allow direct correlation to reported results for electrochemical performance of steel in general, when both alkaline environment and carbon-based additives are concerned. Next, the model solution of pH 13.9 referred to simulating concrete pore water at early stages (in the range of hours) of cement hydration, whereas the solution of pH 12.8 simulated the concrete pore water at later stages of cement hydration.

6.2 Experimental Materials and Methods

6.2.1 NMCSs Preparation and Characterization

NMCSs were obtained through self-polymerization of dopamine (DA) and spontaneous co-assembly of PS-b-PEO di-block copolymer micelles, forming PDA/PS_{173}-b-PEO_{170} composite spheres. The micelles of high molecular weight block polymer PS_{173}-b-PEO_{170} acted as a sacrificial pore-forming agent and were subsequently removed during a carbonization process, leaving mesopores in the range of 5–16 nm in the carbon spheres [20].

Figure 6.1 shows a TEM image and hydrodynamic radius distribution of the as received of the NMCSs, as obtained after carbonization of the PDA/PS-b-PEO at 800 °C. All NMCSs showed relatively rough surface, however, presenting uniformly distributed surface features with an average sphere size varying from approx.

Table 6.1 Mortar specimen's designation

Mortar specimens	NMCS/ wt.% (Cement wt.)	F127/ wt.% (mix water wt.)	Ultrasonification/ min	No. of samples
Blank	0	0	0	4
NMCS	0.025	0	5	4
NMCS + F127	0.025	0.1	0	4
F127	0	0.1	0	4

300 to 400 nm, Fig. 6.1 (particles with a minimum size of 187 nm and a maximum size of 610 nm were observed).

6.2.2 Cement-Based Materials

Preliminary studies on the effect of NMCSs on the global performance of cement-based materials were performed in order to account for their hypothesized influence in reinforced concrete systems in view of bulk matrix properties. Compressive strength tests and electrical resistivity measurements were performed on 40 × 40 × 40 mm mortar cubes with admixed 0.025 wt.% NMCSs (with respect to dry cement weight). The mortar specimens were cast using ordinary Portland cement (OPC) CEM I 42.5 N (ENCI, NL), a water-to-cement ratio (w/c) of 0.5 and 1:3 cement-to-sand ratio. The NMCSs were added within mortar casting as NMCSs only or as a mixture of NMCSs + Pluronic F127, where F127 was employed as a dispersing agent. In the former case (NMCSs only), ultrasonication of the mixing water, representing a solution of NMCSs, was employed prior to mixing it with the dry cement powder. In the latter case (NMCSs + F127), the admixtures were just added within mortar casting in the relevant concentrations. Specimens in which only F127 was added to the mortar mixture were an additional, i.e., control case, for comparative purposes to the samples NMCSs + F127, where F127 was a dispersion agent. The designation and details on sample preparation for the mortar specimens are shown in Table 6.1.

The electrical resistivity of mortar was measured using an AC "2-pin method," where the "pins" were brass mesh pieces with dimensions equal to the sides of the mortar cubes [31]. An R-meter was used to record the electrical resistance of the mortar, measured by applying an alternating current of 1 mA at a frequency of 1 kHz. Electrical resistivity was calculated using Ohm's law: $\rho = R.A/l$, where ρ is the mortar resistivity (in Ohm.cm), R is the electrical resistance of mortar (in Ohm), A is the cross section of the mortar cube (in cm^2) and l is the length of mortar (in cm). The electrical resistivity was monitored immediately after casting and up to 36 days of curing. The tested specimens were maintained and covered in the mold during the whole test period (minimizing environmental effects) and were exposed to constant external conditions.

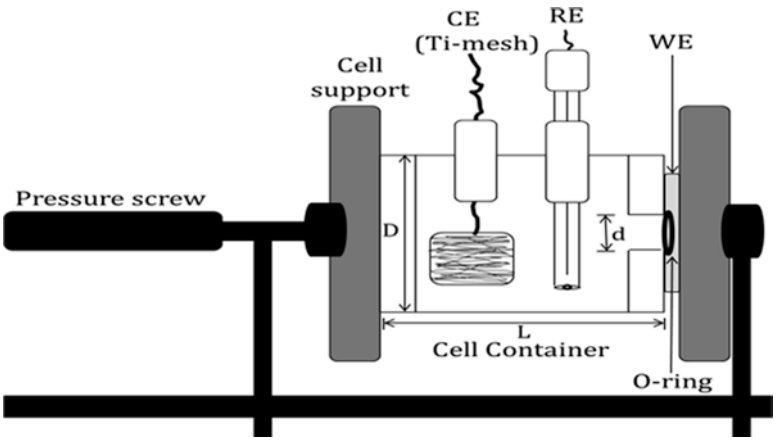

Fig. 6.2 Experimental setup of the three-electrode cell arrangement

Standard compressive strength tests were performed on the 40 × 40 × 40 mm mortar cubes at the hydration age of 36 days. Four replicate mortar specimens were tested.

6.2.3 Steel Electrodes, NMCSs, Model Medium and Sample Designation

Steel electrodes (low carbon St37) with a defined surface area of 0.3 cm^2 were ultrasonically degreased in ethanol, grinded with successive grades of SiC emery paper up to 4000 grade and then polished using 3 and 1 μm diamond paste to mirror-like surface. The electrodes were tested in model solutions of 0.9 M NaOH and 0.1 M NaOH of pH 13.9 and 12.8, respectively, at 25 °C. The electrochemical response of steel in the presence of 0.016% NMCSs was studied in these model solutions, using a flat three-electrode electrochemical cell. The schematic presentation of the employed cell is shown in Fig. 6.2.

Saturated calomel electrode (SCE) was used as a reference electrode, and MMO Ti- mesh as a counter electrode. For each exposure condition, two identical steel specimens (replicates) were tested. Similarly to the cement-based samples, the NMCSs were dispersed in two manners: through ultrasonication or through adding F127 (10 wt.%) as a dispersing agent. The samples designation, corresponding to each studied environment, is given in Table 6.2.

Prior to adding the NMCSs in the relevant solutions, they have been characterized in an identical medium by measuring their Zeta-potential, hydrodynamic radius and particle size distribution, using dynamic light scattering (DLS). The morphology of the NMCSs after carbonization was observed by a transmission electron microscope (JEM-2010).

Table 6.2 Test solution composition and sample designation

NaOH conc. M	pH	NMCS wt.%	F127 wt.%	Designation
0.1	12.8	0	0	A1
		0.016	0	A2
		0	10	A3
		0.016	10	A4
0.9	13.9	0	0	B1
		0.016	0	B2
		0	10	B3
		0.016	10	B4

6.2.4 Electrochemical Methods

Electrochemical measurements were employed to follow up the progressive changes in the electrochemical response of the steel electrodes in control conditions (no additives to the model medium) and in the presence of NMCSs and F127 during 3 days of exposure. The open circuit potential (E_{OCP}) was monitored at different intervals. Electrochemical impedance spectroscopy (EIS) was carried out using Metrohm Autolab-Potentiostat PGSTAT30. EIS measurements were recorded under potentiostatic control at OCP, from 10 kHz down to 10 mHz. An AC perturbation voltage signal of 10 mV (rms) amplitude was applied.

Periodic measurements of the polarization resistance (R_p) were carried out by potentiodynamic measurements from −20 mV to +20 mV versus OCP, at a scan rate of 10 mV/min. The corrosion current density (i_{corr}) was calculated by using the Stern-Geary eq. [32], $i_{corr} = B/R_p$, where B is the Stern-Geary constant. A value of $B = 26$ mV, for active carbon steel, was used and 52 mV for passive steel [33, 34].

At the end of the test, the specimens were subjected to cyclic voltammetry (CV). Ten CV cycles were performed from −1.2 V vs SCE to +0.9 V vs SCE, to cover all reduction and oxidation processes of interest, form hydrogen evolution to water oxidation and oxygen evolution. The scan rate was 1 mV/s.

6.3 Results and Discussion

6.3.1 NMCSs Characterization

The results from DLS and Zeta-potential measurements for the NMCSs in different model solutions (identical to those used for electrochemical tests later on) are listed in Table 6.3. In alkaline environment of pH 13.9 (0.9 M NaOH) and 12.8 (0.1 M NaOH), the average NMCSs particle size varied from 296 to 187 nm, respectively.

In alkaline solution with pH 12.8 and 13.9 (0.1 M and 0.9 M NaOH), the addition of 10% F127 was considered sufficient to ensure the formation of F127 micelles at

Table 6.3 Characterization of NMCSs in alkaline media

Test solution	pH	Zeta potential / mV[a]		DLS / nm
		1st	2nd	
0.9 M NaOH + NMCSs + F127	13.9	1.7	2.1	296
0.1 M NaOH + NMCSs + F127	12.8	1.3	0.98	187

[a]Two measurements were performed in two solutions of the same composition

room temperature, especially in solutions with pH 13.9 [35]. In addition to the possible adsorption of F127 on NMCSs surface, micelles formation was expected to induce additional dispersion of NMCSs in the bulk volume. In solutions of pH 12.8, a clear decrease in the F127 micellization and the adsorption of nonionic surfactant, F127, on NMCSs active surfaces, was reported, which in turn affected dispersion of NMCSs particles. In this case, NMCSs particles with small radius (≈ 187 nm) were easily dispersed; however, bigger aggregates were settled down. In solutions of pH 13.9, the dispersion efficiency was expected to be higher and larger NMCSs particles were dispersed easily in solutions of 0.9 M NaOH. In addition to the expected higher micellization degree of F127 in 0.9 M NaOH solutions, the higher OH^- concentration could lead to more preferential adsorption of OH^- ions on NMCSs. Consequently, NMCSs dispersion and agglomeration, together with higher particle size variation, were expected compared to those in pH 12.8. As reported [36, 37], the critical micelle concentration (CMC) of F127 is strongly dependent on different parameters such as the pH, temperature and ionic strength. Solubility and CMC of F127 strongly decrease as the temperature increases [38, 39]. Additionally, with a pH increase, a reduction in the micelles radius was reported [39].

Pluronic F127 was used in this study as a dispersing agent only. Therefore, evaluating possible effect of F127 on steel electrochemical performance and/or the mortar bulk matrix was not an objective of this work. However, in view of the above considerations, related to behavior of F127 alone, the choice to evaluate it as a separate addition to model solutions, as well as an admixture to mortar, is logic and hence presented in this work for comparative purposes.

Some authors [40–42] argue that nitrogen-adjacent carbon atoms are positively charged and act as active sites for the adsorption of oxygen and/or negatively charged species as OH^-. In alkaline solutions with pH higher than 13, Wan et al. [42, 43] have concluded that the hydroxyl ion sorption on N-doped carbon surfaces proceeded a quick and reversible process. The positive Zeta-potential values of NMCSs are mainly related to positively charged N-atoms. The slight variation in the NMCSs Zeta-potential in solutions of pH 13.9 and 12.8 was probably related to preferential adsorption of cations or anions within the double layer of the active surface [38, 42, 43]. On the other hand, the pH variation induced changes in the nitrogen-oxygen surface active functional groups such as hydroquione-/quinone-like groups in NMCSs [42]. This type of variation of the nitrogen-doped sites on the carbon spheres (Pyridine or Pyrolic N- atoms) is pH-dependent, yielding a considerable change in the chemical state of the functional groups and active sites on the NMCSs,

which causes variation in NMCSs Zeta-potential and average particle size, as listed in Table 6.3.

Considering reported and the hereby observed alterations in charge, size and overall behavior of the NMCSs in the tested model solutions, variations in the passive layer formation on the tested steel surface were expected. Additionally, positive charge of the NMCSs would account for certain limitations on the steel surface in their presence, e.g., positively charged particles can be expected to adsorb on anodic locations (negatively charged in a corrosion cell) and limit the oxidation reactions. Limitations in oxidation, on the other hand, although positive in view of global corrosion resistance development, will impede the passive layer formation and stabilization on the steel surface in the hereby tested environment. Therefore, changes in particles' charge are important in view of the global electrochemical state and will determine the performance of steel in the tested model environment, although steel in alkaline medium (not exceeding pH of 13.7) is expected to be in a passive state. Next to the above and in the case of (reinforced) cement-based materials, the process of cement hydration and distribution of hydration products are expected to be influenced by admixed NMCSs of varying charge. This would be especially the case if early stages of cement hydration are compared to later ages. All these phenomena are not subject to this work and need further in-depth investigation. However, the hereby reported results can be considered preliminary in view of the above aspects and provide an indication for the expected behavior and performance of both steel and cement-based bulk matrix.

6.3.2 Results from Preliminary Tests Bulk Matrix Properties

As aforementioned, reinforced cement-based material can be subjected to certain modification, e.g., by introducing admixtures to the bulk cementitious matrix, investigating the global material properties of the modified bulk material and the corrosion resistance of embedded steel is of equal importance. This is especially the case when an admixture aims to simultaneously affect the concrete microstructural properties (e.g., porosity, permeability and resistivity) and the corrosion resistance of embedded steel, with the final goal to achieve a reinforced concrete system of a superior performance. To that end, a sequence of studies is normally to be followed, before the optimum choice for tests in reinforced concrete is determined. For example, the admixtures are tested for their effect on cement-based bulk matrix only in plain (nonreinforced) specimens, whereas their effect on steel electrochemical response is tested in simulated aqueous environment [33, 43, 44]. In that manner the contribution of many effects in a system of high heterogeneity, as reinforced concrete, is separately evaluated. Therefore, with respect to this work, preliminary tests on global material properties of mortar specimens were performed, when admixtures as the hereby discussed NMCSs were involved.

Electrical resistivity measurements of 40 × 40 × 40 mm cubic mortar specimens were employed as a rapid nondestructive testing method that allows investigating

Table 6.4 Electrical resistivity of mortar cubes at curing time intervals from 0.5 to 36 days

	Electrical resistivity / Ω.cm			
Curing time/ d	Blank	NMCS	NMCS + F127	F127
0.5	142	138	188	174
1	270	271	327	307
5	546	410	963	764
10	1159	878	2012	1618
20	1456	1119	2218	1889
36	1577	1394	2679	2152

Table 6.5 Compressive strength of mortar specimens with different additives after 36 days curing

Mortar specimens	Maximum strength / MPa	
	Mean value	Stand. Dev.
Blank	40.9	3.1
NMCS	54.3	3.9
NMCS + F127	11.5	2.5
F127	16.8	1.6

the quality of the mortar properties. The variations in the electrical resistivity of different mortar specimens with and without 0.025 wt.% NMCSs at different curing time and age respectively are listed in Table 6.4.

As expected, the electrical resistivity increases with cement hydration and age for all tested specimens. What can be noted is that the early properties of the cement-based bulk matrix containing NMCSs are possibly significantly altered. This is reflected by lower electrical resistivity of NMCSs-modified mortar cubes, especially pronounced from initial stages (0.5–5 days) and further until 20 days. At the end of the testing period, 36 days of age, the NMCSs-containing mortar cubes maintained the lowest electrical resistivity values among all tests groups – Table 6.4. In contrast, the highest resistivity values were recorded for mortar cubes where NMCSs were admixed together with F127. This can be attributed to (i) increased cement hydration and densification of the bulk matrix or (ii) decreased ionic mobility in the pore water, blocking of connected pore network paths and/or altered water balance in the presence of nonionic F127. These will end up in changing the process of cement hydration and could have a negative or positive effect, e.g., retardation or acceleration of cement hydration and pore network development, formation of insulated pore space (e.g., air-filled voids). Since the presence of only F127 results in slightly lower electrical resistivity values, compared to NMCSs + F127 (Table 6.4), F127 alone is most likely not responsible for the observed highest electrical resistivity in specimens, containing F127 and NMCSs together.

Additionally, if electrical resistivity values are correlated to compressive strength development (Table 6.5), the influence of admixtures can be judged in terms of global material properties development.

As can be observed in Table 6.5, significantly lower compressive strength was recorded for the mortar matrix, containing F127 alone or F127 together with NMCSs, i.e., in the range of 12–17 MPa compared to 41 MPa for the control case. This result is in contradiction with the higher values of recorded electrical resistivity (Table 6.4) for those two cases, considering the general perception that higher electrical resistivity accounts for a denser matrix, whereas a denser or more matured cement-based material would have a higher compressive strength. Next to that, the specimens containing NMCSs only exhibit the highest compressive strength – 54 MPa. However, these specimens show the lowest electrical resistivity values. In the case of NMCSs alone, the opposite trends of electrical resistivity and compressive strength development can be explained with increased conductivity of the matrix due to the presence of NMCSs, being a carbon-based material of high conductivity as an intrinsic property. The highest compressive strength, though, would be rather related to phenomena linked to cement hydration and formation and/or (re) distribution of calcium-silicate hydrates.

Apparently, competing mechanisms of altered cement hydration, nucleation effects and/or redistribution of hydration products, connected and disconnected pore network, play a role in the development of the cement-based microstructure when both NMCSs and F127 are present. These aspects need further in-depth investigation, which was not subject to the present work. For the purposes of this study, the recorded global material properties are sufficient to justify the selection of the investigated admixtures and their concentration respectively, in order to account for corrosion tests in reinforced mortar and the objective of simultaneous steel corrosion control and improved bulk matrix characteristics. To that end, and at this stage, it can be concluded that the NMCSs would possibly result in superior properties of a reinforced concrete system. However, F127 might not be the best and suitable option as a dispersing agent for the carbon spheres, if the hereby discussed results for compressive strength and electrical resistivity development are considered.

6.3.3 Electrochemical Performance of Steel in the Presence of NMCSs

6.3.3.1 Open Circuit Potential (OCP) and Corrosion Current Density (i_{corr})

The open circuit potential (OCP) and the corrosion current density (i_{corr}) of carbon steel have been monitored in the course of 3 days of continuous exposure to 0.1 M (pH 12.8) and 0.9 M (pH 13.9) NaOH solutions; the obtained data are displayed in Fig. 6.3.

In 0.1 M NaOH solutions (samples A1–A4), more anodic OCP values were measured and i_{corr} stabilized at low current densities after 72 h of immersion in this alkaline medium (Fig. 6.3a, b). This variation in OCP and i_{corr} is related to the formation of electrochemically stable passive film. Similar mechanisms would hold for

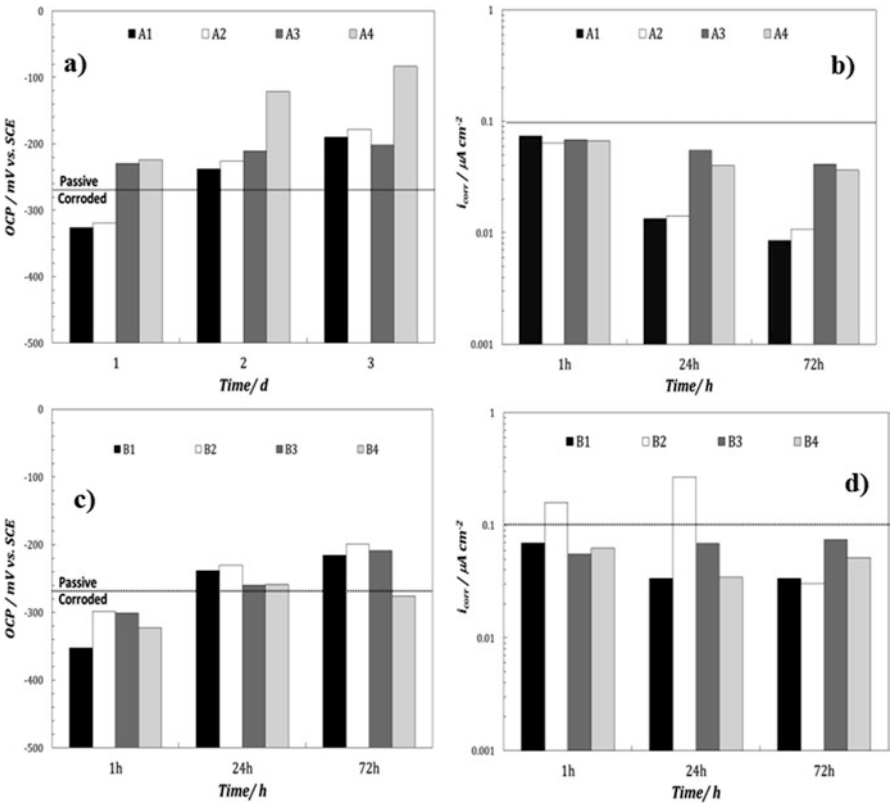

Fig. 6.3 Variation of the open circuit potential (OCP) and corrosion current density (i_{corr}) of the tested steels immersed in 0.1 M NaOH (solutions A) and 0.9 M NaOH (solutions B) after 1, 24 and 72 h. **a**, **c**) E_{corr}, and **b**, **d**) i_{corr}

the steel tested in 0.9 M NaOH environment (solutions B), although more cathodic OCP values were recorded for these specimens, accompanied by slightly higher corrosion current densities (Fig. 6.3c, d). This was as expected due to the aggressiveness of solutions B towards steel, i.e., pH 13.9 is a medium where carbon steel would present active state until passive layer formation will overcome active oxidation. For specimens A1 and A2, the recorded anodic shift in OCP and low i_{corr} values with treatment in 0.1 M NaOH solutions followed the generally expected trend of steel passivation in alkaline medium of pH 12.8. This is due to the gradual development of an oxide film on the surface, as also reported [45–47]. An OCP shift to more anodic values generally reflects a passive film acquiring a stable thickness over time [48]. The addition of 0.016% NMCSs without F127 (solution A2) did not significantly affect the passive film development on the steel surface, i.e., specimens A2 showed similar response to the steel in solutions without additives (A1), with only slight variations in OPC and i_{corr} values. The more noble potential of A2, compared to A1, Fig. 6.3a, would account for a generally improved corrosion resistance.

However, the i_{corr} values as derived for A2 were slightly higher than those for A1 (Fig. 6.3b). The variation between A1 and A2 solutions could be assigned to the effect of NMCSs on the oxygen reduction reaction, resulting in competing mechanisms of passive layer growth on the one hand and catalyzed reduction, i.e., enhanced overall oxidation rate, on the other hand. While the former will account for the establishment of a stable passive state, the latter will lead to increase of the overall corrosion current density. This mechanism is independent from the possible adherence of NMCSs (positive charge) to anodic locations (negatively charged) and effect on the anodic reaction itself. Overall, enhanced reduction, together with blocked anodic areas would result in higher corrosion activity, since more time will be needed for the development of an electrochemically stable and uniform passive film. Therefore, the corrosion activity of A2 ends up slightly higher than that for A1, although a clear trend towards an electrochemically stable passive state was observed, based on OCP and i_{corr} evolution (Fig. 6.3a, b).

The response of specimens A3 and A4 showed a clearly different trend. In both cases, although OCP exhibited ennoblement with time of treatment, especially for the case of A4 (Fig. 6.3a), higher corrosion current was recorded, compared to A1 and A2 (Fig. 6.3b). Obviously, the presence of F127 in both A3 and A4 cases was responsible for the observed behavior. The presence of F127 only, specimen A3, hindered the passive film formation. This is reflected by almost constant OCP values for A3 throughout the test, i.e., substantial ennoblement was not recorded as would otherwise reflect improvement of passivity. The trend of this OCP evolution for A3 was in line with the nonsignificant trend of current density decrease (Fig. 6.3b), i_{corr} values remaining almost one order higher than those for A1 and A2 at the end of the test. The effect of F127 can be also observed for the case of A4 specimens, where despite the very noble OCP values (Fig. 6.3a), the current densities were, similarly to A3, higher than those for A1 and A2 cases. In case of A4 specimens, competitive mechanisms were involved, where the positive effect of NMCSs was counterbalanced by F127. In other words, enhanced oxygen reduction and initially blocked active areas on the steel surface (NMCSs effect), otherwise resulting in a faster development of a stable layer, were counteracted by the presence of F127 (inducing barrier effect); F127 blocked the steel surface, resulting in noble potentials but a nonstable electrochemical state and impeded formation of a passive film. Therefore, in the case of specimens A4 the higher anodic shift in OCP and high i_{corr} values, compared to A1 and A2 solutions, were denoted to a possible formation of an adsorbed layer of nonionic F127 triblock copolymer containing NMCSs on the steel surface. This layer was actually as observed by ESEM examination, as will be presented further below.

The OCP values for steel treated in solution of 0.9 M NaOH (pH of 13.9), (Fig. 6.3c, d), were more cathodic than those in solution of 0.1 M NaOH (pH of 12.8). This was as expected due to the initially more active steel surface at the higher pH, as thermodynamically justified.

For specimens B1 and B2 similar OCP values were measured, while corrosion current densities were higher in the presence of NMCSs, i.e., for B2 (Fig. 6.3c, d). This was related to the effect of NMCSs, inducing high catalytic activity for oxygen

reduction and subsequently enhanced oxidation rate. Once the film developed on the steel surface, the corrosion activity in B2 was reduced, ending up with even lower i_{corr} values, compared to B1 (Fig. 6.3d). The increased corrosion resistance of B2 was reflected by more noble potentials at the end of the test, compared to all other cases (Fig. 6.3c).

Similarly to the A samples, blocking the steel surface was relevant for the F127-containing B samples as well, specimens B3 and B4. Both OCP and i_{corr} records account for reduced corrosion resistance in B3 and B4 samples. The responsible mechanisms here were analogical to those described for specimens A, however, even more pronounced due to the higher corrosivity of the medium, i.e., pH 13.9.

The effect of pH only on the steel electrochemical response, and passive film formation, respectively, can be clearly observed by the comparison of OCP and i_{corr} values of the treated steel in 0.1 M NaOH (A1) and 0.9 M NaOH (B1) solution. In alkaline solutions of pH 13.9 (B1), higher i_{corr} values were registered. It is well known [47–50] that the reduction of Fe^{3+} to Fe^{2+} generally constitutes an additional cathodic reaction, which would affect both OCP and i_{corr} values. The contribution of Fe^{2+} species was expected to be more evident when the potential of the passive film shifted to more negative values [50]. Consequently, the high i_{corr} values in 0.9 M NaOH solutions can be mainly related to the accumulation of Fe^{2+} species within the passive film. However, when the film is exposed to solutions of pH 12.8, which is the case of 0.1 M NaOH solution (A1) in this work, more anodic OCP and lower i_{corr} values would be mainly related to enrichment of the passive film in Fe^{3+} oxides/hydroxides [49, 50].

In the presence of 0.016% NMCSs + 10% F127 (B4), the presence of positively charged NMCSs would limit the Fe^{2+} to Fe^{3+} oxidation, which in turn will lead to increasing the Fe^{2+}-oxide species. This explains the more cathodic potential measured in case of B4 solutions. This cathodic shift in OCP was not observed in solutions B3 with only F127.

6.3.3.2 Electrochemical Impedance Spectroscopy (EIS): Qualification of Response

Electrochemical impedance spectroscopy (EIS) was performed for the tested steel in 0.1 M NaOH (designation A) and 0.9 M NaOH (designation B) solutions and samples respectively. The EIS response in a Nyquist plot format for all specimens, treated in the relevant solutions with and without additives, is presented in Figs. 6.4 and 6.5. In 0.1 M and 0.9 M NaOH solutions without additives (A1 and B1), the limit of impedance values at the low frequency range increases with immersion time, reflecting the spontaneous passivation of steel in alkaline media, Figs. 6.4a and 6.5a. The response in 0.9 M NaOH, Fig. 6.5a, depicts lower corrosion resistance (lower global impedance |Z| values) in accordance with the expected effect of solutions of pH > 13.7, i.e., steel in more active initial state for cases B, compared to medium of pH 12.8, cases A, where only passivity stabilization would be relevant. These observations are in line with the recorded evolution of OCP and i_{corr} for

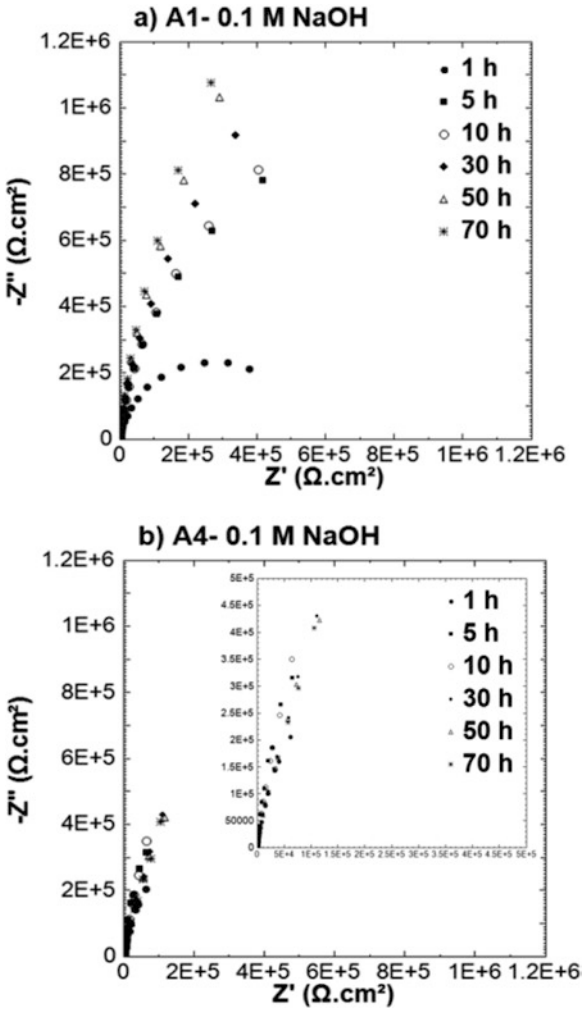

Fig. 6.4 EIS response of St37 after 1, 5, 10, 30, 50 and 70 h of immersion at pH 12.8 in solutions A1 and A4

specimens in solutions A1 and B1 with time of treatment, Fig. 6.3a, c. The EIS results also confirm the previously discussed hypothesis for a more electrochemically stable passive film in conditions of pH 12.8, resulting from predominance of Fe^{3+} species. Furthermore, the higher stability of the passive layer on the steel surface in A1 conditions is evident from the already more pronounced increase of impedance magnitude towards the end of the test (50–70 h) if compared to the EIS response for steel in solution B1 – compare responses for A1 and B1 in Figs. 6.4a and 6.5a.

If the EIS response of steel treated in solutions containing 0.016 wt.% NMCSs +10% F127 (solutions A4 and B4) is compared to additives-free solutions (A1 and B1), the main observations are as follows: the overall impedance in case of solutions A4 was lower than that for additives-free solutions in the same medium (A1) –

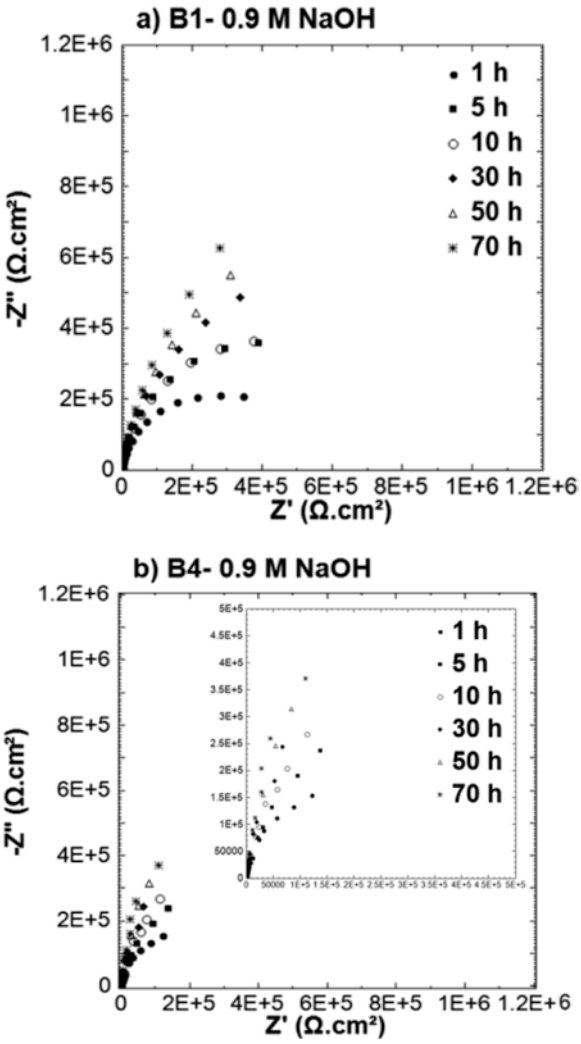

Fig. 6.5 EIS response of St37 after 1, 5, 10, 30, 50 and 70 h of immersion at pH 13.9 in solutions B1 and B4

Fig. 6.4a, b. Furthermore, no increase in the overall impedance with treatment in solution A4 was observed, where the limit of global impedance at the low frequency range remained almost constant after 10 h and until the end of the test (Fig. 6.4b). The observed response accounts for possible limitations within the passive film formation, development and stabilization in the case of A4, which is obviously related to the presence of both NMCSs + F127. The almost constant EIS response for A4 throughout the test reflects a state of counterbalanced diffusion limitation (barrier effect of F127) and passive layer formation. This is in line with the previously discussed simultaneous action of positive NMCSs effect and negative F127 effect, which resulted in OCP ennoblement but a delay in a stable passive film formation.

In the case of the B4 samples, the originally higher steel activity in 0.9 M NaOH solutions impeded the barrier effect of F127 and altered the action of NMCSs. The result was a nonstable response over time, with a gradual increase in global magnitude of impedance. The corrosion resistance of B4, however, remained lower than that for the B1 specimens (Fig. 6.5a, b). Here again, the addition of NMCSs + F127 limited the development of a stable passive film, although the relevant mechanism was entirely different from that in solutions A4. In both cases where particles were present – A4 and B4, the overall impedance ends up lower compared to particles free solutions – A1 and B1. This is well in line with the recorded corrosion current densities towards the end of the test (Fig. 6.3b, d, where the corrosion current densities for steel in solutions A4 and B4 were higher than these for steel, treated in solutions A1 and B1.

Figure 6.6a, b depicts the Nyquist diagrams of the impedance spectra for all tested steel specimens at the end of the test. In 0.1 M NaOH (pH 12.8) – solutions A1 and A2, the addition of 0.016% NMCSs showed nonsignificant effect on the impedance response (Fig. 6.6a). For steel treated in the presence of F127 only, specimens A3, a less capacitive behavior compared to solutions A1 and A2 was observed. This decrease in the overall impedance of the tested steels in solutions A3 is related to retardation in passive film formation, induced by diffusion limitations at the steel/solution interface in the presence of F127. A mixed charge transfer/mass transfer mechanism of the electrochemical reaction in A3 is evident by the depression (distortion) of the semicircular response of A3 in the low frequency domain (Fig. 6.6a, showing an initial capacitive-like response, followed by inclination of the curve to the real axis). On the other hand, in case of steel treated in solutions A4 with NMCSs +10% F127, relatively higher impedance than in case of A3 solutions was measured, Fig. 6.6a. This is reflected by the more pronounced capacitive-like behavior of A4 (response inclined to the imaginary axis) which is also in agreement with the more noble OCP values, measured for A4, compared to A3 at the same exposure conditions, Fig. 6.3a. Since for A4 the competition of passive layer formation (at pH 12.8 and NMCSs effect) counteracted the limitations to stable passivity (F127 affect), the global magnitude of |Z| ends up higher than that for A3, but lower than A1 and A2. The result is well in-line with the recorded corrosion current density from LPR method (Fig. 6.3b).

Regarding 0.9 M NaOH solutions (pH 13.9), the tested B specimens (B1–B4) showed a relatively lower overall impedance, when compared to A-specimens. The comparison of the steel EIS response for B1 and B2 cases indicated that, the addition of 0.016% NMCSs (B2 solution) induced a decrease in impedance compared to the B1-solution, Fig. 6.6b. Concerning EIS response of the immersed steel in B4 solution, more resistive behavior than in B1, B2 solutions, was observed, while low impedance values were derived in the case of F127 only, i.e., specimens B3. This trend for B3 is similar to that obtained in A3 solution, Fig. 6.6a, b. The effect of NMCSs and F127 together (B4) was again seen in the increase of corrosion resistance, compared to F127 alone (B3). In contrast to A4 specimens, the effect of NMCSs + F127 together, as in B4 specimens in medium of pH 13.9, was more pronounced and not entirely in line with the results in Fig. 6.3b, c, where cathodic

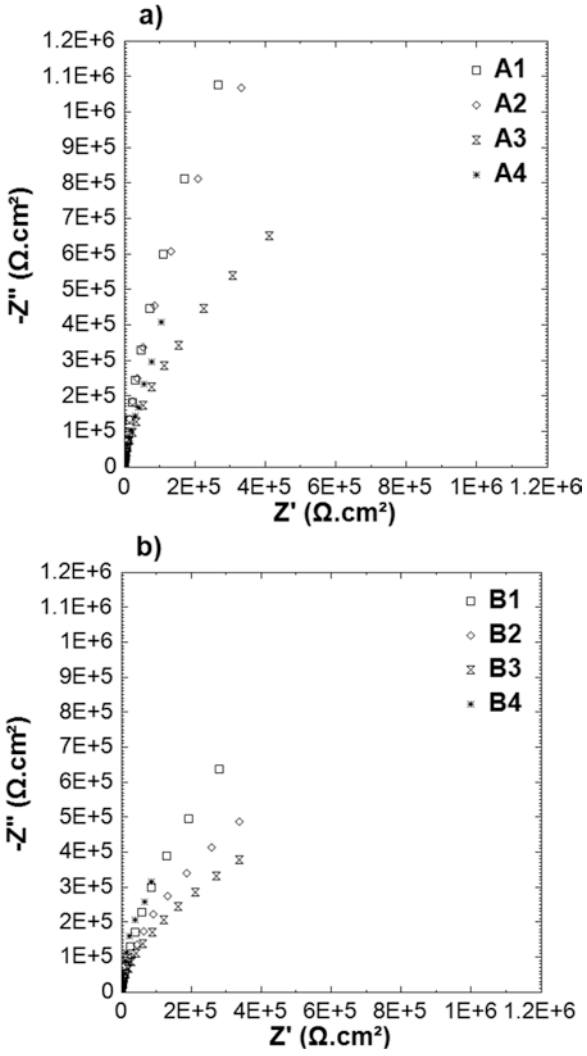

Fig. 6.6 Nyquist plots for St37 after 70 h of immersion in all tested solutions

values for B4 were recorded. However, as previously discussed, the OCP for B4 remained almost constant at the later stages of the test. This was discussed to be related to a hold-back of stable passive film formation due to limitations at the steel/solution interface in the presence of F127, on one hand, and enhanced redox activity due to the presence of NMCSs and the higher pH of the B solution, on the other hand. Hence, although similar response was monitored in case of A4 solutions, the nature of the mechanisms involved in A4 and B4 are different, as also reflected by both electrochemical response and surface properties (presented further below). The reason behind these observations is related to the effect of pH on F127 itself, together with the effect of pH on the dispersion of the NMCSs. These transforma-

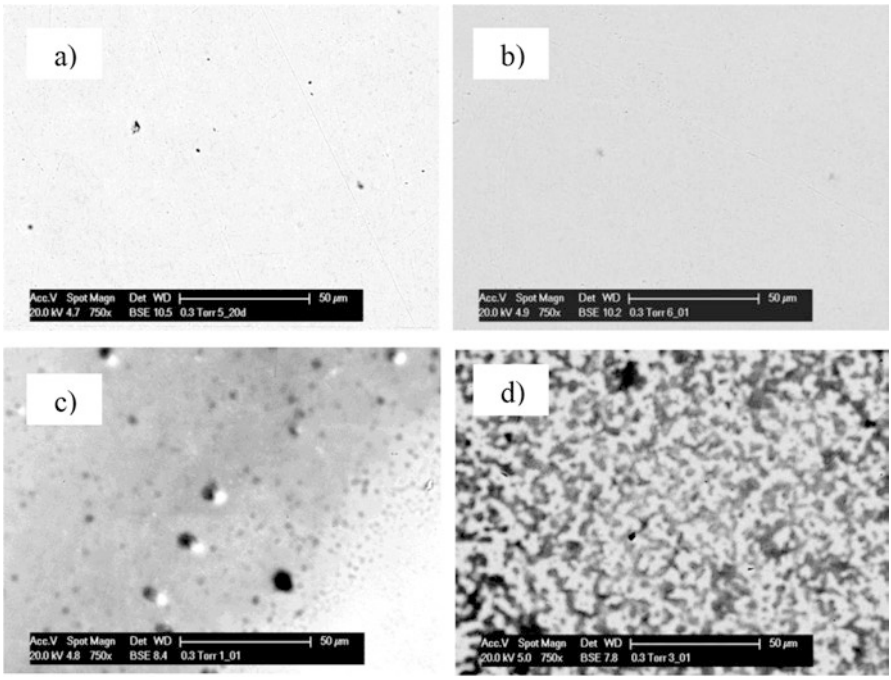

Fig. 6.7 ESEM images of St37 after 70 h treatment: (**a**) A1, (**b**) B1, (**c**) A4 and (**d**) B4

tions, although potentially of high importance in view their effect on electrochemical state, were not subject to this work. What can be clearly stated, though, is that at pH of 12.8, the NMCSs particles in the bulk of the solution, and presumably adjacent to the steel surface, were of a smaller size (approx. 200 nm), while the dispersed particles in pH 13.9 were larger – approx. 300 nm (Table 6.3).

The particle size distribution is perhaps a large contributing factor to the observed electrochemical response. Smaller particles exhibit larger surface area. This, together with the previously introduced electrocatalytic, etc. properties of NMCSs, will logically and irrespective of all other factors determine the oxidation/reduction reactions on the steel surface. These reactions would be facilitated in specimens A and would result in a faster stabilization of passivity, if compared to specimens B – which was as observed. Clearly, a more in-depth investigation on the interactions of NMCSs, with and without F127, with the steel surface is needed in order to confirm or reject the above hypothesis.

The above discussed phenomena with regard to passive film formation, or limitations thereof, together with the recorded EIS response, i_{corr} and OCP, are well in line and supported by microscopic examination of the steel surface at the end of the test. The visual observation (via electron microscopy) reveals the relatively clean surface for steel treated in additives-free solutions – A1 and B1, Fig. 6.7a, b. In contrast, the appearance of steel treated in A4 and B4 solutions varies significantly, Fig. 6.7c, d. In the former case (A4 solutions), the steel surface appears to be smooth and in

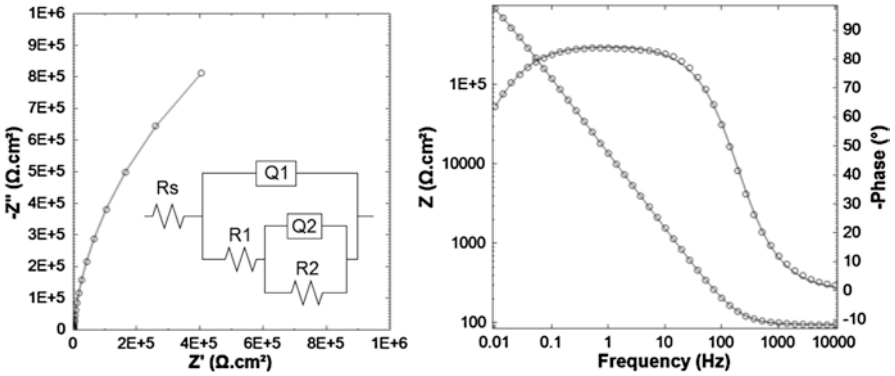

Fig. 6.8 EIS response obtained for carbon steel after 10 h of immersion in A1-solution (0.1 M NaOH). Experimental data (*dots*) and fitting (*solid line*), using the equivalent circuit $R_e(R_1Q_1(R_2Q_2))$, where $R_e = 96\Omega$, $R_1 = 621\ k\Omega\ cm^2$, $Q_1 = 5.1 \times 10^{-5}$, $n = 0.94$, $R_2 = 211\ k\Omega\ cm^2$, $Q_2 = 1.7 \times 10^{-5}$, $n = 0.9$, and $\chi^2 = 0.005$

similar to A1 condition with the difference of randomly distributed particles, obviously adhering to the substrate. In the latter case (B4), the steel surface appears to be covered by a dense composite layer, containing both NMCSs and F127.

6.3.3.3 EIS Response: Brief Intro to Quantification

The recorded EIS response for all investigated cases was discussed in the previous sections in view of qualification of electrochemical state. Qualitative interpretation of EIS data is possible and well accepted as an approach, providing a rapid evaluation of the overall corrosion resistance for the tested systems. The quantitative evaluation of EIS is relatively more complex. This is in view of the necessity to account for exact physical meaning and discuss in detail the relevant electrical parameters used within fitting of the experimental data. This type of quantification is not subject to this work. An introduction to the quantification of the recorded EIS response is provided only, together with the derived polarization resistance (R_p) values from EIS as an AC method. The objective was to provide a comparison with R_p values derived from DC electrochemical tests in view of evaluating the global corrosion state of the tested specimens.

Figure 6.8 presents the EIS response, fit and equivalent electrical circuit employed for a steel specimen treated in A1-solution after 10 h of conditioning. Figure 6.8 is representative for all investigated cases. The best-fit parameters were derived by using an equivalent electrical circuit of two hierarchically arranged time constants in series with the electrolyte resistance, i.e., $R_e(R_1Q_1(R_2Q_2))$, where Re is the solution resistance; the high frequency time constant ($R_1 \cdot Q_1$) is associated with the charge transfer resistance and pseudo-double layer capacitance; the low frequency time constant ($R_2 \cdot Q_2$) is related to the redox transformations, mainly Fe^{2+}/Fe^{3+}, in

the surface layer [44, 51, 52]. The replacement of pure capacitance with a constant phase element (Q) is largely accepted in literature [44, 51] because of inhomogeneities at different levels, i.e., steel surface roughness, product layer heterogeneity, etc. The global polarization resistance (R_p) values can be derived from EIS via simplification, using the relation of $R_p = R_1 + R_2$ [44]. A good agreement between the model and the experimental data was found, reflected by acceptable error per element and for the overall fit of the full response (Fig. 6.8).

The comparison of the global polarization resistance, R_p, measured from DC measurement (LPR) and the one, derived from EIS is shown in Fig. 6.9a, b. The R_p values measured by EIS data were higher than those recorded via LPR. Experimentally, the polarization resistance measurements were done at 4 mHz (±20 mV around OCP at 10 mV/min), below the lowest frequency limit considered for EIS measurements (10 mHz) [53, 54]. Thus, the measured R_p form DC measurements are affected by both R_1 and R_2 parameters, which are related to the charge transfer resistance and redox processes, which occurred in the passive film layer, respectively. The deviations in the R_p measurements by EIS and DC method are more relevant after 72 h immersion in both 0.1 and 0.9 M NaOH, A and B solutions. This is related to the employment of different electrochemical AC and DC techniques in case of EIS and LPR, respectively.

It should be mentioned that both the R_p values measured by EIS or DC techniques were reproducible and similar variation trends in parallel exposure conditions was observed Fig. 6.9a, b.

In additive free solutions, A1 and B1, the polarization resistance of the tested steels in these solutions was improved by aging, as shown in Fig. 6.9a, b. Furthermore, in agreement with the aforementioned results (Figs. 6.3 and 6.5), the measured resistance in B1 solutions was relatively lower than in case of A1 solutions. This was related to the pH effect on the grown passive film of the treated steels in additive-free A1 and B1 solutions.

The tested steels in solutions A2 and B2, in the presence of NMCSs, showed similar R_p values to those measured in case of solutions A1 and B1, respectively, Fig. 6.9a, b. In 0.1 M NaOH solutions with 10% F127 (solutions A3), the R_p values showed nonsignificant variation after 24 h of immersion. These results confirm that the passive film formation was hindered in the presence of F127 at the steel/solution interface. On the other hand, the presence of NMCSs with F127 (solution A4) resulted in a slight increase in R_p values, observed after 72 h, Fig. 6.9a. Concerning the tested steels in B4 solutions, the R_p values shows similar variation trend to B1 and B2 solutions, reaching almost the same R_p values after 72 h aging, Fig. 6.9b. These results were not as the observed results in solutions A4, where the R_p showed no significant variation after 24 h, Fig. 6.9a. This can be explained in regards to the variation in dispersed NMCSs properties in B4 solutions, where the NMCSs was expected to be preferentially adsorbed on the anodic zones due to the variation in the NMCSs charge density (Table 6.3). In B4 solutions with pH 13.9, the anodic zones are expected to be more dense than in the case of A4 solutions (pH 12.8). This could explain the visual changes of the adsorbed layer on the steel surface immersed in A4 and B4 detected by ESEM observation, shown in Fig. 6.7c, d.

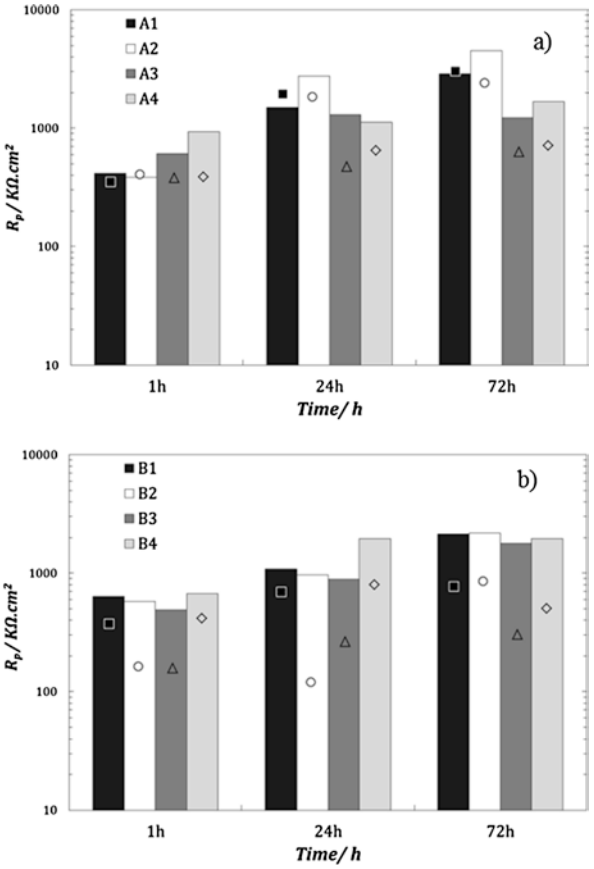

Fig. 6.9 Comparison of the polarization resistance, R_p, measured by DC and AC methods (LPR and EIS): (**a**) 0.1 M NaOH solutions (A1–A4) and (**b**) 0.9 M NaOH solutions (B1–B4) after 1, 24 and 72 h. *Column*: R_p from EIS; *Symbols*: R_p from LPR

6.3.3.4 Cyclic Voltammetry (CV)

Carbon steel behavior in 0.1 and 0.9 M NaOH solutions of different pH, with and without NMCSs, was analyzed by performing CV after 3 days of immersion.

Figure 6.10a, b present the voltammograms corresponding to the last cycle of the tested carbon steel in 0.1 M NaOH solution (A1 and A4) and 0.9 M NaOH solutions (B1and B4), respectively. Three potential domains can be clearly distinguished: iron redox process domain, passivation region and oxygen evolution, Fig. 6.10a, b.

In the forward scan, the main iron activity peak appeared E ≈ −0.75 V vs SCE (peak I) was assigned mainly to magnetite formation [46, 55, 56]. Then, the current was maintained almost constant along the passivity domain (from −0.4 to +0.5 V) until reaching the oxygen evolution potential, E ≈ 0.55 V vs SCE (peak II). Fliz et al. [56] have indicated that at potential above −0.4 V vs SCE, the potentiodynamically grown passive film did not contain ferrous compounds and it mainly contained $Fe(OH)_3$ and/or FeOOH.

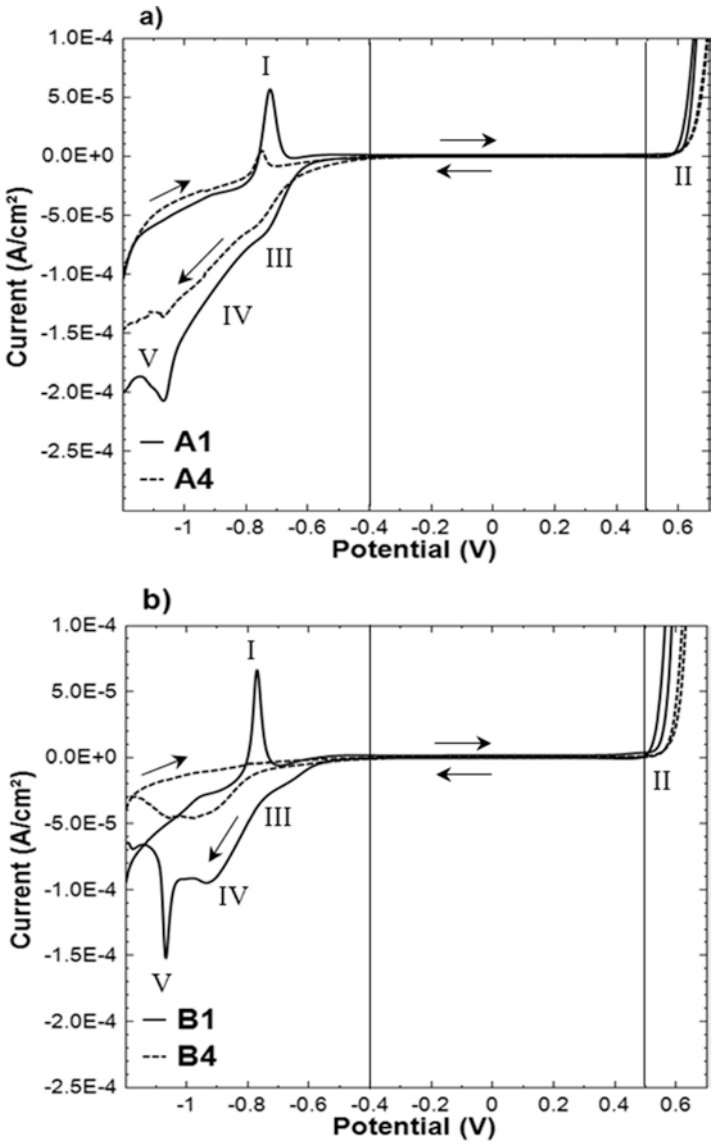

Fig. 6.10 Comparison of the 10th cycles of carbon steels after 3 days of immersion in (**a**) 0.1 M NaOH solution (A1–A4) and (**b**) 0.9 M NaOH (B1–B4)

In the cathodic scan, the formed iron oxide species reduced at three different cathodic potentials assigned as peaks III, V and IV, which corresponded to the reduction of Fe^{3+} species, Magnetite and Fe^{2+} species, respectively [46].

By comparing the cyclic voltammograms in solutions A1 and B1, a cathodic shift in peak I in solution B1 of pH 13.9 was monitored with respect to the same peak

appearing in case of solution A1. Furthermore, the cathodic current densities associated to peaks III, IV and V were relatively higher in case of A1 solution when compared to solution B1, as shown in Fig. 6.3.

If solutions with additives (A4 and B4) are compared to solutions without additives (A1 and B1), a very well pronounced difference was observed for both 12.8 and 13.9 solutions. A clear decrease of the current densities associated to anodic and cathodic peaks was monitored. In addition, the anodic and cathodic peaks assigned to iron activity peaks were shifted to more cathodic potentials when compared to additive-free solutions (A1 and B1, respectively). The oxygen evolution peaks in case of solutions A4 and B4 were slightly shifted to more anodic potentials, reflecting the variation of steel/adjacent solutions interface properties in the presence of additives, compared to additives-free cases, Fig. 6.10.

In A4 solutions, the addition of 10% F127 + 0.016% NMCSs induced a clear decrease in peak I current with shift to more cathodic potential. Moreover, the cathodic current densities of the appeared peaks were lower than in case of A1 solution. In agreement with R_p data shown in Fig. 6.9a, this fact can explain the reason of nonsignificant variation in R_p in case of steel immersed in A4 solution. Mainly, because of the expected formation of less oxidized passive film with potentially lower magnetite content in the presence of 10% F127 + 0.016% NMCSs. In addition, a limited reduction process was observed in case of A4 solution, which confirms the possible blocking of the cathodic sites. This blocking did not induce additional barrier properties because of its effect on the passive film chemical composition.

In case of the treated steels in B4 solutions, the presence of 10% F127 + 0.016% NMCSs caused a drastically lower anodic and cathodic activity peaks. This decrease in the iron activity peaks resulted from the formation of an adsorbed layer on the surface of the treated steel in B4 solutions, confirmed by surface examination using ESEM (Fig. 6.7d). In this case, the formed layer on the steel treated in solutions B4 induced additional barrier properties, which in turn explain the relatively high R_p values in the case of B4 solutions, especially after 1 and 24 h, Fig. 6.9b. However, after 3 days, similar R_p values to the control samples (B1) were monitored, which was higher than in case of A4-solutions, Fig. 6.9.

Fundamentally, the passive film has been described to have a bilayer structure, which consists of inner layer of Fe_3O_4 and an outer layer of γ- Fe_2O_3 [47, 52–57]. According to the point defect model (PDM), the passive film is a highly doped but graded defect semiconductor structure, in which the vacancies are assumed to act as the electronic dopants. The donor vacancy in the oxide films were Fe^{2+} interstitials and/or oxygen vacancies, and the former is the major donor since the rate of consumption is higher than the its generation [58–59]. The acceptor vacancies were the cation vacancies on cation sub-lattice in the barrier layer [58–59]. Based on the CV data, the mechanism of the potentiodynamically formed passive film could be explained as follows: at low potential (more cathodic than −0.7 V vs SCE), Fe_3O_4 was the main constituent of the passive film with relatively small amount of γ-Fe_2O_3 [57]. As the potential increased above −0.5 V vs SCE, more and more Fe_3O_4 was anodically converted to γ- Fe_2O_3 and γ- FeOOH [57].

The presence of NMCSs in the oxide/solution interface could play an important role in regulation of the electronic properties of the passive layer and its chemical composition. The presence of the carbon-based material in the passive film interface showed a tendency to accept the excess electrons from oxygen vacancies [60]. Therefore, the passive film formed in the presence of NMCSs was expected to have higher Fe^{2+} interstitials and/or oxygen, which is in agreement with the cathodic shift in peak I in solutions A4. Consequently, less γ- Fe_2O_3 and γ- FeOOH content would be related to A4, compared to the control cases (A1 solutions). The higher the carrier density, the greater is the passive film conductivity [60, 61]. Consequently, this increase in the conductivity led to a decreasing value of passive film R_p, compared to the additive-free case, which was in accordance with the measurements shown in Fig. 6.9. Furthermore, this can explain the decrease in the current densities associated to the anodic and the cathodic peaks, as appearing in the cyclic voltammograms in the presence of NMCSs, Fig. 6.10.

The treated steel samples in solutions B4 showed more pronounced blocking of the steel surface, where higher anodic current from the iron activity domain was measured. No clear oxidation peaks were observed. In the cathodic scan, the limitations of the NMCSs highly affected the iron oxide species reduction processes, because of the catalytic effect of NMCSs on oxygen reduction at the expense of iron reduction processes.

6.4 Conclusions

The electrochemical response of carbon steel in 0.1 and 0.9 M NaOH was controlled by the induced variation in the NMCSs properties, together with the pH value of the surrounding media. In alkaline solutions with pH 12.8, the presence of NMCSs at the steel/solution interface induced the formation of passive film with comparable to control conditions impedance magnitude. The fact was mainly related to the competition of passive layer formation and destabilization induced by the blockage of active areas on the steel surface by NMCSs.

In 0.9 M NaOH solutions (pH 13.9), the tested steels in B-solutions (B1–B4) showed a relatively lower overall impedance, when compared to A-solutions with pH 12.8. In the presence of NMCSs particles, a competing mechanism of active state, i.e., enhanced oxidation on the one hand, and particles adsorption on anodic sites and oxidation limitation, on the other hand, was relevant inducing larger fluctuations in impedance response and stabilization only towards the end of the testing period.

The use of F127 as a dispersion agent is not a suitable option for NMCSs in alkaline media due to its effect in limiting the passive film growth by the formation of an adsorbed layer on the steel surface.

Mortar bulk matrix properties were highly affected by NMCSs and F127. Lowest electrical resistivity values were monitored in mortar specimens mixed-in with only 0.025 wt.% NMCSs, which would result in better conduction of electrical current

flow. However, the presence of F127 induces an increase in the electrical resistivity.

The addition of 0.025 wt.% NMCSs (with respect dry cement weight) improves the compressive strength. Nevertheless, the compressive strength of mortar specimens with F127 or NMCSs + F127 was three times lower than the control specimens. This decrease in compressive strength in the presence of F127 can be explained as the natural consequence of a progressive weakening of the matrix, probably caused by increasing porosity and/or hindering the cement hydration in the presence of nonionic F127.

References

1. Bertolini L, Elsener B, Pedeferri P, Polder R (2004) Corrosion of steel in concrete: prevention, diagnosis, repair, 1st edn. Wiley, Weinheim, pp 71–121
2. American Concrete Institute (1985) Committee 222, corrosion of metals in concrete. ACI J 81:3–32
3. Broomfield JP (2007) Corrosion of steel in concrete: understanding, investigation and repair. Spons Architecture Price Book, London
4. Balaguru PN, Shah SP (1992) Fiber reinforced cement composite. McGraw-Hill Inc., New York
5. Kowald T (2004) Influence of surface modified carbon nanotubes on ultra-high performance concrete. In: Schmidt M, Fehling E (eds) Proceedings international symposium on ultra-performance concrete. Kassel University Press GmbH, pp 195–202
6. Angst U, Elsener B, Larsen KC, Vennesland Ø (2009) Critical chloride content in reinforced concrete – a review. Cem Concr Res 39:1122–1138
7. Chernin L, Val DV (2011) Prediction of corrosion-induced cracking in reinforced concrete structures. Constr Build Mater 25:1854–1869
8. Lui Y, Weyers RE (1998) Modelling the time to corrosion cracking in chloride contaminated reinforced concrete structures. ACI Mater J 95:675–681
9. Koleva DA, de Wit JHW, van Breugel K, Lodhi ZF, van Wesring E (2007) Investigation of corrosion and cathodic protection in reinforced concrete. J Electrochem Soc 154:52–61
10. Mahmoud H, Alonso MC, Sanchez M (2012) Service life extension of concrete structures by increasing the chloride threshold using stainless steel reinforcements. In: Alexander MG et al (eds) Concrete repair, rehabilitation and retrofitting III. Taylor & Francis Group, London, pp 497–503
11. Pan Z, He L, Qiu L, Korayem AH, Li G, Zhu JW, Collins F, Li D, Duan WH, Wang MC (2015) Mechanical properties and microstructure of a graphene oxide-cement composite. Cem Concr Compos 58:140–147
12. Collins F, Lambert J, Duan WH (2012) The influence of admixtures on the dispersion, workability, and strength of carbon nanotuble-OPC past mixtures. Cem Concr Compos 34:201–207
13. Jo BW, Kim CH, Tea GH, Park JB (2007) Characteristics of cement mortar with nano-SiO2 particles. Constr Build Mater 21:1351–1355
14. Refait P, Jeannin M, Sabot R, Antony H, Pineau S (2013) Electrochemical formation and transformation of corrosion products on carbon steel under cathodic protection in seawater. Corros Sci 71:32–36
15. Carmona J, Garcés P, Climent MA (2015) Efficiency of a conductive cement-based anodic system for the application of cathodic protection, cathodic prevention and electrochemical

chloride extraction to control corrosion in reinforced concrete structures. Corros Sci 96:102–111
16. Duwell EJ, Todd JW, Butzke HC (1964) The mechanism of corrosion inhibition of steel by ethynylcyclohexanol in acid solution. Corros Sci 4:435–441
17. Yang W, Li Q, Xiao Q, Liang J (2015) Improvement of corrosion protective performance of organic coating on low carbon steel by PEO pretreatment. Prog Org Coat 89:260–266
18. EN 1990 (2002) Eurocode- basis of structural design. European Committee for Standardization, Brussels
19. Sanchez F, Sobolev K (2010) Nanotechnology in concrete- a review. Const Build Mater 24:2060–2071
20. Tang J, Liu J, Li C, Li Y, Tade MO, Dai S, Yamauchi Y (2014) Synthesis of nitrogen-doped mesoporpous carbon spheres with extra-large pores through assembly of diblock copolymer micelles. Angew Chem Int Edn 53:588–593
21. Yang T, Liu J, Zhou R, Chen Z, Xu H, Qiao SH, Monterio M (2014) N-doped mesoporous carbon shperes as the oxygen reduction catalysts. J Mater Chem A 2:18139–18146
22. Zhang LL, Gu Y, Zhao XS (2013) Advanced porous carbon electrodes for electrochemical capacitor. J Mater Chem A 1:9395–9408
23. Parveen S, Rana S, Fangueiro R (2013) A review on nanomaterial dispersion, microstructure and mechanical properties of carbon nanotube and nanofiber reinforced cementitious composites. Nanomaterials 2013:1–19
24. Yazdenbakhsh A, Grasley Z (2012) The theoretical maximum achievable dispersion of nanoinclusions in cement paste. Cem Concr Res 42:798–804
25. Konsta-Gdoutos MS, Metaxa ZS, Shah SP (2010) Highly dispersed carbon nanotube reinforced cement based materials. Cem Concr Res 40:1052–1059
26. Peng H, Alemany LB, Margrave JL, Khabashesku VN (2003) Sidewall carboxylic acid functionalization of single-walled carbon nanotubes. J Am Chem Soc 125:15174–15182
27. Xin X, Xu G, Zhao T (2008) Dispersing carbon nanotubes in aqueous solutions by a starlike block copolymer. J Phys Chem C 112:16377–16384
28. Bystrzejewski M, Huczko A, Lange H, Gemming T, Büchner B, Rümmeli MH (2010) Dispersion and diameter separation of multi-wall carbon nanotubes in aqueous solutions. J Colloid Interface Sci 345:138–142
29. Liao YH, Marietta-Tondin O, Liang Z, Zhang C, Wang B (2004) Investigation of the dispersion process of SWNTs/SC-15 epoxy resin nanocomposites. Mater Sci Eng A 385:175–181
30. Li J, Li Z, Tong J, Xiaa C, Li F (2015) Nitrogen-doped ordered mesoporous carbon sphere with short channel as an efficient metal-free catalyst for oxygen reduction reaction. RSC Adv 5:70010–70016
31. Susanto A, Koleva DA, Copuroglu O, van Beek K, van Breugel K (2013) Mechanical, electrical, and microstructural properties of cement-based materials in condition of stray current flow. J Adv Concr Technol 11:119–134
32. Stern M, Geary AL (1957) A theoretical analysis of the shape of polarization resistance curves. J Electrochem Soc 104:56–63
33. Andrade C, Alonso C (1996) Corrosion rate monitoring in the laboratory and on-site. Constr Build Mater 10:315–328
34. Zornoza E, Paya J, Garces P (2008) Chloride-induced corrosion of steel embedded in mortars containing fly ash and spent cracking catalyst. Corros Sci 50:1567–1575
35. Basak R, Bandynopadhyay R (2013) Encapsulation of hydrophobic drugs in pluronic F127 micelles: effect of drug hydrophobicity, solution temperature, and pH. Langmuir 29:4350–4356
36. Eliseeva OV, Besseling NAM, Koopal LK, Cohen Stuart MA (2005) Influence of NaCl on the behavior of PEO-PPO-PEO triblock copolymers in solutions, at interface, and in asymmetric liquid films. Langmuir 21:4954–4963

37. Eliseeva OV, Fokkink RG, Besseling NAM, Koopal LK, Cohen Sturat MA (2006) Thinning of wetting films formed from aqueous solutions of non-ionic surfactant. J Colloid Interface Sci 301:210–216
38. Nita LE, Chiriac AP, Bercea M (2012) Effect of pH and temperatura upon self-assembling process between ploy(aspartic acid) and pluronic F127. Colloid Surf B Biointer 119:6539–6545
39. Alexander S, de Vos WM, Castle TC, Cosgrove T, Prescott SW (2014) Growth and shrinkage of pluronic micelles by uptake and release of flurbiporfen: variation of pH. Langmuir 28:47–57
40. Gong K, Du F, Xia ZH, Durstock M, Dai LM (2009) Nitrogen-doped carbon nanotube arrays with high Electrocatalytic activity for oxygen reduction. Science 323:760–764
41. Deng DH, Pan XL, Yu LA, Cui Y, Jiang YP, Qi J, Li WX, Fu QA, Ma XC, Xue QK, Sun GQ, Bao XH (2011) Toward N-doped graphene via solvothermal synthesis. Chem Mater 23:1188–1193
42. Wan K, Yu ZP, Li XH, Liu MY, Yang G, Piao JH, Liang ZX (2015) pH effect on electrochemistry of nitrogen-doped carbon catalyst for oxygen reduction reaction. Catalysis 5:4325–4432
43. Koleva DA, Denkova AG, Boshkov N, van Breguel K (2013) Electrochemical performance of steel in cement extract and bulk matric properties of cement past in presence of pluronic 123 micelles. J Mater Sci 48:2490–2503
44. Hu J, Koleva DA, de Wit JHW, Kolev H, van Breugel K (2011) Corrosion performance of carbon steel in simulated pore solutions in presence of micelles. J Electrochem Soc 158:C76–C87
45. Diaz B, Joiret S, Keddam M, Novoa XR, Perez MC, Takenouti H (2004) Passivity of iron in mud's water solution. Electrochim Acta 49:3039–3048
46. Joiret S, Keddam M, Novoa XR, Perez MC, Rangel C, Takenouti H (2002) Use of EIS, ring-disk electrode, EQCM and Raman spectroscopy to study the film of oxides formed on iron in 1M NaOH. Cement Concr Comp 24:7–15
47. Freire L, Nóvoa XR, Montemor MF, Carmezim MJ (2009) Study of passive films formed on mild steel in alkaline media by the application of anodic potentials. Mater Chem Phys 114:962–972
48. Alonso C, Andrade C, Izquierdo M, Novoa XR, Perez MC (1998) Effect of protective oxide scales in macrogalvanic behavior of concrete reinforcement. Corros Sci 40:1379–1389
49. Antony H, Legrand L, Marechal L, Perrin S, Dillmann P, Chausse A (2005) Study of lepidorcrocite γ-FeOOH electrochemical reduction in natural and slightly alkaline solutions at 25 °C. Electrochem Acta 51:745–753
50. Freire L, Carmezima MJ, Ferreiraa MGS, Montemora MF (2010) The passive behaviour of AISI 316 in alkaline media and the effect of pH: a combined electrochemical and analytical study. Electrochim Acta 55:6174–6181
51. Koleva DA, Boshkov N, van Breugel K, de Wit JHW (2011) Steel corrosion resistance in model solutions, containing waste materials. Electrochim Acta 58:628–646
52. Andrade C, Merino P, Nóvoa XR, Pérez MC, Soler L (1995) Passivation of reinforcing steel in concrete. Mater Sci Forum 192-194:891–898
53. Mahmoud H, Sanchez M, Alonso MC (2015) Ageing of the spontaneous passive state of 2304 duplex stainless steels in high-alkaline conditions with the presence of chloride. J Solid State Electrochem 19:2961–2972
54. Andrade C, Keddam M, Novoa XR, Perez MC, Rangel CM, Takenouti H (2001) Electrochemical behavior of steel rebars in concrete: influence of environmental factors and cement chemistry. Electrochim Acta 46:3905–3912
55. Abreu CM, Covelo A, Daiz B, Freire L, Novoa XR, Perez MC (2007) Electrochemical behavior of iron in chlorinated alkaline media; the effect of slurries form granite processing. J Braz Chem Soc 18:1156–1163
56. Flis J, Oranowska H, Smialowska ZS (1990) An ellipsometric study of surface films grown on iron and iron carbon alloys in 0.05 M KOH. Corros Sci 30:1085–1099

57. Li WS, Luo JL (1999) Electronic properties and pitting susceptibility of passive films on ferrite and pearlite in chloride-containing solution. Proc Electrochem Soc 27:161–170
58. Macdonald DD (1992) The point defect model for passive state. J Electrochem Soc 139:3434–3449
59. Castro EB (1994) Analysis of the impedance response of passive iron. Electrochim Acta 39:2117–2123
60. Liu L, Xu J, Xie ZH, Munroe P (2013) The roles of passive layers in regulating the electrochemical behaviour of Ti_5Si_3-based nanocomposite films. J Mater Chem A 1:2064–2078
61. Xia Y, Cao F, Liu W, Chang L, Zhang H (2013) The formation of passive films of carbon steels in borate buffer and their degradation behavior in NaCl solution by SECM. Int J Electrochem Sci 8:3057–3073